

# Stochastic Optimization of Medium- and Short-term Reserve Arrangement for Preventive and Emergency Control Under Typhoon Disaster

Yunchu Wang, *Student Member, IEEE*, Yusheng Xue, *Fellow, IEEE*, Dongliang Xie, Yuge Chen, Changming Chen, and Zhenzhi Lin, *Senior Member, IEEE*

**Abstract**—With the increase in the permeability of renewable energy and the frequency of extreme weather, the power system requires a large amount of flexible power regulation capacity. In order to realize the multi-day cooperation of reserve resources, the stochastic optimization of medium- and short-term reserve arrangement considering the typhoon uncertainty is studied in this paper. Firstly, the extreme scenario generation and reduction method considering the typhoon path–intensity prediction uncertainty is constructed. Then, considering the combined cost of preventive and emergency control for adequacy in multiple scenarios, the reserve arrangement optimization model in extreme weather is built. In this model, the pre-dispatching strategies for multiple types of reserve resources are proposed to maintain the medium- and short-term coordination. Finally, case studies on a simplified 24-node power system of Zhejiang province, China are presented based on the data of the typhoon Fireworks in July 2021, and the result shows that the proposed reserve arrangement optimization model can reduce the total cost of power systems and the risk of operation under the typhoon disaster.

**Index Terms**—Reserve arrangement, typhoon uncertainty, preventive control for adequacy, emergency control for adequacy, stochastic optimization, risk-based coordination.

## I. INTRODUCTION

**I**N recent years, the penetration rate of renewable energy in power systems has been increasing, and the impact of extreme weather on the security and stability of power systems has risen, requiring stronger flexible power regulation capabilities [1], [2]. At present, the power system reserve is mainly provided by thermal units, but the thermal units are

slow to start and have many constraints on ramping up/down, as well as the minimum technical output limitations. Therefore, the coordination of the thermal units and the rapidly adjustable reserve resources such as energy storages and demand-side resources is the key to balancing the security, economy, and low-carbon operation requirements of the renewable energy generation dominated power system [3], [4].

The probability and frequency of low-probability high-loss events rise during extreme weather, and the shortage of reserve resources leads to insufficient adequacy of the power system, thus threatening the security of the power system. Meanwhile, before the predictable extreme weather, the power system operator has enough time to schedule the flexible resource reserves and emergency plans over a long timescale [5], [6]. Typhoon, as common extreme weather in coastal areas, has the characteristics of a long impact period, high uncertainty, and violent changes before and after transit. There is often a deviation between the predicted and actual moving paths. Meanwhile, the pre-stages, mid-stages, and late stages of typhoon weather have different impacts on the power system. For example, high uncertainty and low power loads in the pre-stages and mid-stages of typhoon extreme weather require simultaneous improvement of power system up-regulation and down-regulation capacities, while rapid load recovery after typhoons requires high power system up-regulation capacity. Therefore, advanced control of power system reserve resources and multi-day coordinated scheduling is required, and the short-term (day-ahead and real-time) power system scheduling may lead to insufficient power system adequacy during extreme weather. In [7]–[9], to deal with the generation operation adequacy problem in the renewable energy generation dominated power system, the power system adequacy control is divided into three periods according to the control timing, which are the preventive control for adequacy (PCfA) before the occurrence of the adequacy event, the emergency control for adequacy (ECfA) at the beginning of the event, and the correction control shared with the security and stability control. In [10], considering the uncertainty of the possibility of high-risk events with a small probability such as extreme weather, a self-dispatching model of power generation enterprises based on the conditional value at risk is proposed to improve the expected profit of power generation enterprises. In [11], a sequentially proactive operational

Manuscript received: April 1, 2024; revised: May 27, 2024; accepted: June 8, 2024. Date of CrossCheck: June 8, 2024. Date of online publication: July 5, 2024.

This work was supported by the Science and Technology Project of NARI Technology Co., Ltd. “Interaction and Coordination Technology of Information–Physical–Social Elements” (No. GF-GFWD-210338).

This article is distributed under the terms of the Creative Commons Attribution 4.0 International License (<http://creativecommons.org/licenses/by/4.0/>).

Y. Wang, Y. Chen, C. Chen, and Z. Lin are with the College of Electrical Engineering, Zhejiang University, Hangzhou 310027, China (e-mail: wangyunchu\_ee@zju.edu.cn; cheniyuge@zju.edu.cn; changmingchen@zju.edu.cn; linzhenzhi@zju.edu.cn).

Y. Xue (corresponding author) and D. Xie are with the NARI Group Corporation (State Grid Electric Power Research Institute), Nanjing 211106, China (e-mail: xueyusheng@sgepri.sgcc.com.cn; xiedongliang@sgepri.sgcc.com.cn).

DOI: 10.35833/MPCE.2024.000353



strategy is proposed to enhance the resilience against extreme-weather-triggered cascading failures, and typhoons are utilized as typical weather disaster scenarios to study resilience decisions during extreme weather. In [12], a three-stage day-ahead resilient unit commitment model that considers uncertain typhoon paths and line outages is proposed to improve the power system resilience against typhoon events. In [13], a resilience method against typhoon for integrated electricity and natural gas distribution systems is proposed, where the multi-stage stochastic model based on a scenario tree is utilized to address the uncertain moving paths of the typhoon. The above work has studied the power system resilience under typhoon disasters. However, the reserve arrangement of power systems is taken as the fixed value in the upper and lower limit constraints, lacking the assessment and collaborative optimization of the medium- and short-term reserve under typhoon disasters, and consideration of the impact of typhoon prediction uncertainty on sources and load.

In recent years, three main reserve arrangement optimization models have been proposed considering the output uncertainty of renewable energy sources. Firstly, the deterministic model mostly uses a certain proportion of capacity of a unit or a certain proportion of load as the reserve, which is widely used in power systems [14], [15]. However, it cannot meet the reserve requirements when various operating conditions of the renewable energy generation dominated power system change. In the probabilistic model based on probability density [16], the renewable energy source, demand-side load, thermal unit outage, and other uncertain factors are modeled using probability distribution function, and the reserve arrangement is obtained by combining the loss of load probability and the value of lost load (VOLL) [17]. The computational load associated with probabilistic methods based on probability density is relatively low, but it has difficulties coping with high-risk events with low probability such as extreme weather [18]. Furthermore, the probabilistic model based on the scenario method usually uses Monte Carlo simulation and other scenario generation methods to obtain uncertain scenarios of renewable energy source and load, and an reserve arrangement optimization model is built with the goal of minimizing the expected cost of multiple scenarios. In [19], an assessment of flexibility reserves in stochastic modeling at day-ahead and real-time timescales is presented. In [20], a stochastic bi-level program to compute reserve requirements in sequential markets is proposed, which implicitly improves the inter-temporal coordination of energy and reserve markets. In [21], [22], a methodology for probabilistic zonal reserve arrangement is proposed to address wind power prediction uncertainties. The impacts of generation and reserve on carbon emissions are analyzed in [23], [24], and a multi-period optimization model for coordinating the generation, carbon capture, and reserves is proposed considering the cost of carbon emissions. In [25], a multi-stage strategy integrating multi-level decentralized reserve is proposed for resilience enhancement in electricity-gas integrated energy systems. The thermal units, energy storages, and demand-side reserve (DSR) resources are taken as the primary, secondary, and tertiary reserves, respectively. The reserve ar-

range optimization models considering the impacts of economic, carbon emissions, and risks of power systems are built in the above research, but the timescales of these models are day-ahead or real-time without considering the long-term coordination of reserve resources on a weekly or monthly basis.

Given this background, a medium- and short-term reserve arrangement optimization model for multiple types of reserve resources considering the typhoon uncertainty is proposed in this paper. The major contributions of this paper can be summarized as follows.

1) The stochastic optimization model of medium- and short-term reserve arrangement under typhoon disasters is proposed. In the model, the impact of typhoon uncertainty on factors (in generation, load, and grid sides) related to reserve arrangement is fully considered, which can coordinate the arrangement of different reserve resources under extreme weather to obtain a lower combined cost of PCfA and ECfA than other models.

2) The reserve arrangement optimization models considering the pre-dispatching of fuel consumption, initial state of charge (SOC), and interruption times are constructed for multiple types of reserve resources, respectively, to realize the spatio-temporal coordination of the electricity reserve and capacity reserve of each resource on a longer time scale.

3) Considering the typhoon path-intensity prediction uncertainty, the extreme scenario generation and reduction method based on the double probability circle model is proposed, which describes the uncertainty of renewable energy sources and electricity load under the typhoon disaster, and reduces the risk of power systems during extreme weather.

## II. SCENARIO GENERATION CONSIDERING TYPHOON UNCERTAINTY

The power system reserve arrangement should ensure the adequacy for both general and extreme operating scenarios, and the medium- and short-term scenarios should be generated in the context of the multi-day typhoon. Therefore, medium- and short-term typical scenarios and extreme scenarios are generated and reduced considering source and load fluctuations under typhoon disaster in this section.

### A. Typhoon Path-Intensity Uncertainty Set Based on Double Probability Circle Model

The strong nonlinear characteristics in the development and evolution of typhoons such as atmospheric movement lead to errors that cannot be ignored in the path and intensity prediction of typhoons. The National Meteorological Center of China Meteorological Administration, the Joint Typhoon Warning Center, the Japan Meteorological Agency, and other meteorological prediction centers all use the ensemble prediction model to generate the probability prediction map of typhoon path. It is expected that about 60%-70% of the whole tropical cyclone path can be included in the probability range [26], [27]. In this paper, the uncertainty set of the typhoon path is generated based on the double probability circle model, which can more comprehensively cover

the possible scenarios, and the set samples are highly representative [28]. Four extreme typhoon paths are distributed on each probability circle, which are fast-paced, slow-paced, leftward-biased, and rightward-biased, as shown in Fig. 1. At the same time, each path corresponds to three scenarios of the maximum, weaker, and moderate wind speeds of typhoon, and corresponds to the error values of 90%, 50%, and 10% of the cumulative probability curve of the maximum wind speed error, respectively. There are a total of 27 typhoon uncertainty scenarios in the typhoon path-intensity uncertainty set.

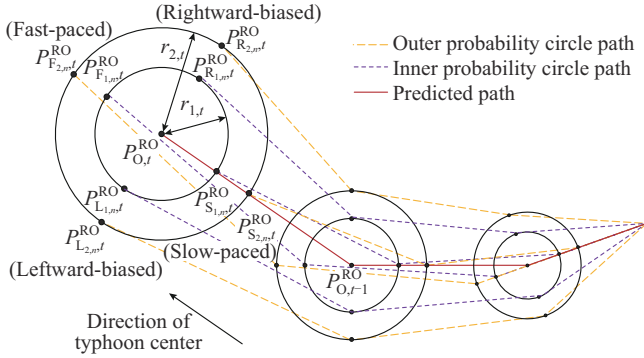


Fig. 1. Typhoon path based on double probability circle model.

The center position of each typhoon path can be calculated by the predicted center  $P_{O,t}^{RO}$  and the radius of the probability circle  $r_{m,t}$  ( $m=1,2$ ). The maximum wind speed of the typhoon can be calculated based on the maximum wind speed of the prediction center  $V_{O,t}^{\max}$  and the correction factor  $\beta_n^V$  ( $n=1,2$ ).  $m$  and  $n$  are the probability circle location and typhoon intensity of the typhoon path, respectively. For the rightward-biased and stronger typhoon located in the outer probability circle, the typhoon center position  $P_{R_{2,1,t}}^{RO}(x_{R_{2,1,t}}^{RO}, y_{R_{2,1,t}}^{RO})$  and the maximum wind speed  $V_{R_{2,1,t}}^{\max}$  can be expressed as:

$$\begin{cases} x_{R_{2,1,t}}^{RO} = x_{O,t}^{RO} + r_{2,t}(y_{O,t}^{RO} - y_{O,t-1}^{RO})/D_{O,t}^{RO} \\ y_{R_{2,1,t}}^{RO} = y_{O,t}^{RO} - r_{2,t}(x_{O,t}^{RO} - x_{O,t-1}^{RO})/D_{O,t}^{RO} \\ V_{R_{2,1,t}}^{\max} = V_{O,t}^{\max} \beta_1^V \end{cases} \quad (1)$$

$$D_{O,t}^{RO} = R_E \arccos(\sin(y_{O,t}^{RO})\sin(y_{O,t-1}^{RO}) + \cos(y_{O,t}^{RO})\cos(y_{O,t-1}^{RO})\cos(x_{O,t}^{RO} - x_{O,t-1}^{RO})) \quad (2)$$

where  $D_{O,t}^{RO}$  is the moving distance of the predicted typhoon center at time  $t$ ;  $R_E$  is the average radius of the earth (generally 6371 km); and  $(x_{O,t}^{RO}, y_{O,t}^{RO})$  and  $(x_{R_{2,1,t}}^{RO}, y_{R_{2,1,t}}^{RO})$  are the longitude and latitude coordinates of the predicted typhoon center of the typhoon path at time  $t$ , respectively.

In the double probability circle model, each path on the same probability circle has the same probability of occurrence. The probabilities of each path on the inner probability circle and the outer probability circle are  $p_1^r$  and  $p_2^r$ , respectively, and the probability of the central prediction path is  $p_0^r$ . The probabilities of the typhoon with the moderate, weaker, and stronger intensities are  $p_0^f$ ,  $p_1^f$ , and  $p_2^f$ , respectively. Therefore, the typhoon path-intensity uncertainty set based on the double probability circle model can be expressed as:

$$Ty = \{(P_{\omega,t}^{RO}, V_{\omega,t}^{\max}) | p_{\omega} = p_m^r p_n^f\} \quad (3)$$

$$\sum p_{\omega} = 1 \quad \omega \in \{O_{0,n}, R_{m,n}, L_{m,n}, F_{m,n}, B_{m,n}\} \quad (4)$$

where  $Ty$  is the typhoon path-intensity uncertainty set, including the coordinates of the path center  $P_{\omega,t}^{RO}$  and the maximum wind speed  $V_{\omega,t}^{\max}$  of typhoon  $\omega$ ;  $p_{\omega}$  is the probability of typhoon  $\omega$ ; and  $O_{0,n}$ ,  $R_{m,n}$ ,  $L_{m,n}$ ,  $F_{m,n}$ , and  $B_{m,n}$  are the central path, the rightward-biased typhoon path, the leftward-biased typhoon path, the fast-paced typhoon path, and the slow-paced typhoon path, respectively.

In the typhoon environment, the wind speed of each position on the map depends on the spatio-temporal distribution model of typhoon, i.e., the probability circle model of typhoons [29]. The wind speed of position  $P_i(x_{P_i}, y_{P_i})$  can be expressed as the vector sum of the moving wind speed component and the circulating wind speed component, i.e.,

$$\dot{V}_{\omega, P_i, t} = \dot{V}_{\omega, P_i, t}^d + \dot{V}_{\omega, P_i, t}^r \quad (5)$$

where  $\dot{V}_{\omega, P_i, t}$  is the initial wind speed at position  $P_i$  in typhoon  $\omega$  at time  $t$ ; and  $\dot{V}_{\omega, P_i, t}^d$  and  $\dot{V}_{\omega, P_i, t}^r$  are the moving wind speed and circulating wind speed at position  $P_i$ , respectively. There is an internal deflection angle between the circulation wind speed direction and the counterclockwise tangential direction of the circular symmetric wind field, generally taking an approximate value of  $20^\circ$ .

According to Masayuki Miyazaki-Rankine model [30], the moving wind speed and circulating wind speed are expressed as:

$$V_{\omega, P_i, t}^d = V_{\omega,t}^{RO} \exp\left(-\frac{\pi r_{\omega, P_i, t}}{10R_{\omega,t}^{\max}}\right) \quad (6)$$

$$V_{\omega, P_i, t}^r = \begin{cases} V_{\omega,t}^{\max} r_{\omega, P_i, t} / R_{\omega,t}^{\max} & r_{\omega, P_i, t} \in [0, R_{\omega,t}^{\max}] \\ V_{\omega,t}^{\max} R_{\omega,t}^{\max} / r_{\omega, P_i, t} & r_{\omega, P_i, t} \in (R_{\omega,t}^{\max}, \infty) \end{cases} \quad (7)$$

where  $V_{\omega,t}^{RO}$  is the moving wind speed of the typhoon center;  $r_{\omega, P_i, t}$  is the distance between the typhoon center  $(x_{O,t}^{RO}, y_{O,t}^{RO})$  and position  $P_i$ ; and  $R_{\omega,t}^{\max}$  is the maximum wind speed radius.

## B. Scenario Generation and Reduction Under Typhoon Path-Intensity Uncertainty Set

In order to simulate the renewable energy source output and load fluctuation scenarios during the typhoon, it is necessary to simulate the wind speed, solar intensity, precipitation, etc., and judge the generation and load status at different geographical locations.

### 1) Wind Power Output Model

The typhoon has a large impact on the wind speed at the wind farm. When the wind speed exceeds the rated value, the wind turbine maintains its rated power through pitch control. When the wind speed surpasses the cut-out speed, the power of the turbine is reduced to 0 to avoid mechanical damage to the aerogenerator during the typhoon. According to the wind power output characteristics, the relationship between the output of the wind turbine and the wind speed can be expressed as:

$$P_{\varpi, W_i, t} = \begin{cases} 0 & v_{\varpi, P_i, t} \leq v_{W_i}^{\text{in}}, v_{W_i}^{\text{out}} \leq v_{\varpi, P_i, t} \\ P_{W_i}^N (v_{\varpi, P_i, t} - v_{W_i}^{\text{in}}) / (v_{W_i}^N - v_{W_i}^{\text{in}}) & v_{W_i}^{\text{in}} < v_{\varpi, P_i, t} < v_{W_i}^N \\ P_{W_i}^N & v_{W_i}^N \leq v_{\varpi, P_i, t} < v_{W_i}^{\text{out}} \end{cases} \quad (8)$$

where  $P_{\varpi, W_i, t}$  is the power of wind turbine  $W_i$  in typhoon  $\varpi$  at time  $t$ ;  $v_{\varpi, P_i, t}$  is the wind speed at position  $P_i$  in typhoon  $\varpi$  at time  $t$ ;  $v_{W_i}^{\text{in}}$ ,  $v_{W_i}^{\text{out}}$ , and  $v_{W_i}^N$  are the rated wind speed, cut-in wind speed, and cut-out wind speed of wind turbine  $W_i$ , respectively; and  $P_{W_i}^N$  is the rated power of wind turbine  $W_i$ . The uncertainty of wind speed can be described as the Weibull distribution [31], and its probability density function can be expressed as:

$$f(v_{\varpi, P_i, t}) = \frac{P_{\varpi} k_w}{V_{\varpi, P_i, t}^{k_w}} v_{\varpi, P_i, t}^{k_w - 1} \exp\left(-\left(\frac{v_{\varpi, P_i, t}}{V_{\varpi, P_i, t}}\right)^{k_w}\right) \quad (9)$$

where  $k_w$  is the shape parameter of wind speed fluctuation.

### 2) Load Correction Based on Typhoon Mode Judgment

Affected by the suspension of some industries under the typhoon disaster, the electricity load in this area decreases slightly when the typhoon passes through and then increases after that. Therefore, it is necessary to judge the typhoon mode of each node of electricity load in scenarios with different typhoon paths and intensities. The typhoon mode at the electricity node is determined according to the wind speed at that position. When the maximum wind speed of the node on day  $d$  is higher than the threshold value  $v_{\text{ty}}^{\text{max}}$  (generally set to be 17.2 m/s), the electricity load can be considered in typhoon mode. Then, the typhoon mode of that electricity load ends when the wind speed falls below the threshold  $v_{\text{ty}}^{\text{max}}$ . Since the moving speed of the typhoon determines the number of days that affect the node of electricity load, it is assumed that the duration of the mode before and after the typhoon transit is consistent with the duration of the typhoon mode. Therefore, load  $L_i$  at position  $P_i$  can be expressed as:

$$P_{\varpi, L_i, t}^{\text{ty}} = k_{\varpi, P_i, d} P_{L_i, t}^{\text{pre}} \quad (10)$$

where  $P_{L_i, t}^{\text{pre}}$  and  $P_{\varpi, L_i, t}^{\text{ty}}$  are the predicted power and corrected power of load  $L_i$  in typhoon  $\varpi$  at time  $t$ , respectively; and  $k_{\varpi, P_i, d}$  is the correction coefficient of the load at position  $P_i$  on day  $d$ . At the same time, it is generally believed that the power load meets the Gaussian distribution [32], and its probability density function can be expressed as:

$$f(P_{\varpi, L_i, t}) = \frac{P_{\varpi}}{\sqrt{2\pi} \sigma_{L_i}} \exp\left(-\frac{(P_{\varpi, L_i, t} - P_{\varpi, L_i, t}^{\text{ty}})^2}{2\sigma_{L_i}^2}\right) \quad (11)$$

where  $\sigma_{L_i}$  is the variance of the Gaussian distribution of load  $L_i$ .

### 3) Extreme Scenario Generation and Reduction Based on Clustering of Needed Controllable Power (NCP)

Firstly, the scenario set of the NCP can be obtained by sampling the power of wind turbines and electricity load at each node under each typhoon path based on the Latin hypercube sampling [33], which can be expressed as:

$$\begin{cases} \mathbb{S}_0 = \{\mathbb{P}_{N, s} | s = 1, 2, \dots, S_0\} \\ \mathbb{P}_{N, s} = \{P_{N, t, s} | t = 1, 2, \dots, T\} \end{cases} \quad (12)$$

$$P_{N, t, s} = \sum_{i=1}^{N_L} P_{L_i, t, s} - \sum_{i=1}^{N_W} P_{W_i, t, s} \quad (13)$$

where  $\mathbb{S}_0$  is the scenario set of the NCP, where the NCP in scenario  $s$  is expressed as  $\mathbb{P}_{N, s}$ ;  $S_0$  is the total number of scenarios of NCP;  $T$  is the total number of time periods;  $P_{N, t, s}$  is the regulated power at time  $t$  in scenario  $s$ , which can be calculated by the electricity load  $P_{L_i, t, s}$  and power of wind turbine  $P_{W_i, t, s}$ ; and  $N_L$  and  $N_W$  are the total numbers of loads and wind turbines, respectively.

Then, the  $K$ -medoids clustering algorithm is used to divide scenarios into  $K$  categories, and the cluster center of each category can be seen as typical scenarios [34]. In this model, the number of typical scenarios is determined under the condition that the intra-class similarity is higher than the upper limit of clustering convergence decision error [35]. The typical scenario set of reserve arrangement optimization can be expressed as:

$$\mathbb{S}_A = \{\mathbb{P}_{N, s_k}^A | k = 1, 2, \dots, K\} \quad (14)$$

where  $\mathbb{S}_A$  is the typical scenario set of the NCP; and  $\mathbb{P}_{N, s_k}^A$  is the typical scenario in the category  $k$  of the NCP. The probability of each typical scenario is  $(N_k - 1)/S_0$ , and  $N_k$  is the number of scenarios in the category  $k$ .

Since the operation of reserve resources in the power systems should focus on extreme scenarios with the largest fluctuation, the edge points of clustering are utilized as extreme scenarios for reserve arrangement optimization. The scenario with the largest Euclidean distance from each cluster center in the category  $k$  of the NCP can be selected as the extreme scenario. The extreme scenario set for reserve arrangement optimization can be expressed as:

$$\mathbb{S}_E = \{\mathbb{P}_{N, s_k}^E | d(\mathbb{P}_{N, s_k}^E, \mathbb{P}_{N, s_k}^A) = \max d(\mathbb{P}_{N, s_k}, \mathbb{P}_{N, s_k}^A)\} \quad (15)$$

where  $\mathbb{S}_E$  is the extreme scenario set of the NCP;  $\mathbb{P}_{N, s_k}^E$  is the extreme scenario in the category  $k$ ; and  $d(\cdot)$  is the Euclidean distance. The probability of each extreme scenario is  $1/S_0$ .

To sum up, the NCP scenario set  $\mathbb{S}_N$  considering typhoon path-intensity prediction uncertainty is composed of the typical scenario set and the extreme scenario set, and can be expressed as:

$$\mathbb{S}_N = \mathbb{S}_A \cup \mathbb{S}_E \quad (16)$$

$$\sum_{s=1}^{N_s} p_s = 1 \quad (17)$$

where  $N_s$  is the number of scenarios; and  $p_s$  is the probability of scenario  $s$  in the typhoon path-intensity uncertainty set.

### 4) $N-x$ Failure Uncertainty Set of Transmission Lines

A transmission line comprises a set of line segments and towers, which are generally more likely to be subject to the damages of typhoons. In this paper, a long transmission line is equivalent to a series of line segments that are connected via two adjacent transmission towers. Consequently, the equivalent failure probability of a transmission line can be modeled as a series system with several line segments and

towers.

The failure rate and the failure probability of the  $i^{\text{th}}$  tower of transmission line  $km$  at time  $t$  can be expressed as:

$$\vartheta_{\sigma, H_{i, km}, t} = \begin{cases} 0 & v_{\sigma, H_{i, km}, t} \leq v_{H_{i, km}}^d \\ e^{\gamma(v_{\sigma, H_{i, km}, t} - 2v_{H_{i, km}}^d)} & v_{H_{i, km}}^d < v_{\sigma, H_{i, km}, t} \leq 2v_{H_{i, km}}^d \\ 1 & v_{\sigma, H_{i, km}, t} > 2v_{H_{i, km}}^d \end{cases} \quad (18)$$

$$p_{\sigma, H_{i, km}, t} = 1 - e^{-\vartheta_{\sigma, H_{i, km}, t} / (1 - \vartheta_{\sigma, H_{i, km}, t})} \quad (19)$$

where  $\vartheta_{\sigma, H_{i, km}, t}$  and  $p_{\sigma, H_{i, km}, t}$  are the failure rate and the failure probability of the  $i^{\text{th}}$  tower of transmission line  $km$  at time  $t$  in typhoon  $\sigma$ , respectively;  $v_{\sigma, H_{i, km}, t}$  is the wind speed of the  $i^{\text{th}}$  tower of transmission line  $km$  at time  $t$  in typhoon  $\sigma$ ;  $\gamma$  is the model coefficient, which is considered to be 0.2 in this paper; and  $v_{H_{i, km}}^d$  is the designed wind speed of each tower, which is considered to be 35 m/s in this paper [36].

The failure rate  $\vartheta_{\sigma, L_{j, km}, t}$  and the failure probability  $p_{\sigma, L_{j, km}, t}$  of the  $j^{\text{th}}$  line segment of transmission line  $km$  at time  $t$  can be expressed as:

$$\vartheta_{\sigma, L_{j, km}, t} = l_{L_{j, km}} e^{\kappa v_{\sigma, L_{j, km}, t} / v_{L_{j, km}}^d - \beta} \quad (20)$$

$$p_{\sigma, L_{j, km}, t} = 1 - e^{-\vartheta_{\sigma, L_{j, km}, t}} \quad (21)$$

where  $v_{\sigma, L_{j, km}, t}$  is the wind speed of the  $j^{\text{th}}$  line segment of transmission line  $km$  at time  $t$  in typhoon  $\sigma$ ;  $v_{L_{j, km}}^d$  is the designed wind speed of the  $j^{\text{th}}$  line segment;  $l_{L_{j, km}}$  is the length of the  $j^{\text{th}}$  line segment of transmission line  $km$ ; and  $\kappa$  and  $\beta$  are the model coefficients, which are considered to be 11.0 and 18.0 in this paper, respectively [36].

The equivalent failure probability of transmission line  $km$  is assumed to be equal to the aggregated failure probability of all towers and all line segments, which can be obtained by:

$$p_{\sigma, km, t}^{\text{TR}} = 1 - \prod_{j=1}^{N_{L, km}} \prod_{i=1}^{N_{H, km}} (1 - p_{\sigma, L_{j, km}, t}) (1 - p_{\sigma, H_{i, km}, t}) \quad (22)$$

where  $p_{\sigma, km, t}^{\text{TR}}$  is the failure probability of transmission line  $km$  at time  $t$  in typhoon  $\sigma$ ; and  $N_{L, km}$  and  $N_{H, km}$  are the numbers of line segments and towers of transmission line  $km$ , respectively.

Considering the differences of failure probability of the transmission line, the  $N-x$  failure uncertainty set of transmission lines is modeled as:

$$\mathbb{R}^{\text{TR}} = \left\{ \lambda^{\text{TR}} \left| \prod_{km=1}^{N_{\text{TR}}} (p_{\sigma, km, t}^{\text{TR}})^{1 - \lambda_{km, t, s}^{\text{TR}}} \prod_{km=1}^{N_{\text{TR}}} (1 - p_{\sigma, km, t}^{\text{TR}})^{\lambda_{km, t, s}^{\text{TR}}} \geq \partial_{\text{TR}} \right. \right\} \quad (23)$$

$$\lambda_{km, t, s}^{\text{TR}} \in \{0, 1\} \quad (24)$$

where  $\mathbb{R}^{\text{TR}}$  is the uncertainty set of transmission lines;  $\lambda_{km, t, s}^{\text{TR}}$  is the on/off state of transmission line  $km$  at time  $t$  in scenarios  $s$ ;  $N_{\text{TR}}$  is the total number of transmission lines; and  $\partial_{\text{TR}}$  is the uncertainty budget of the maximum line outage [37].

To estimate the worst impact, the transmission line outage model with the objective of maximizing the sum of line failure probability is formulated as:

$$\begin{cases} \max \sum_{km=1}^{N_{\text{TR}}} (1 - \lambda_{km, t, s}^{\text{TR}}) p_{\sigma, km, t}^{\text{TR}} \\ \text{s.t.} \sum_{km=1}^{N_{\text{TR}}} \lambda_{km, t, s}^{\text{TR}} [\lg(1 - p_{\sigma, km, t}^{\text{TR}}) - \lg p_{\sigma, km, t}^{\text{TR}}] \geq \lg \partial_{\text{TR}} - \sum_{km=1}^{N_{\text{TR}}} \lg p_{\sigma, km, t}^{\text{TR}} \end{cases} \quad (25)$$

Then, during the time periods with transmission line outage, the power flow constraints can be constructed based on a piecewise linear AC power flow model [38], which can be found in Supplementary Material A. The DC power flow constraints [39] are applied during time periods without transmission line outage in any scenario.

### III. MEDIUM- AND SHORT-TERM RESERVE ARRANGEMENT OPTIMIZATION CONSIDERING PCFA AND ECFA

Under the extreme weather, the increase in source and load uncertainty will require increased long-term reserve of the system, especially the down-reserve requirement [40]. It is necessary to consider the time complementarity of various resources in different stages of extreme weather. Therefore, a reserve arrangement optimization model considering the PCfA and ECfA of multiple flexible resources is proposed, and the control strategies of PCfA and ECfA in typical and extreme scenarios are shown in Fig. 2, where  $\rho$  is the adequacy.

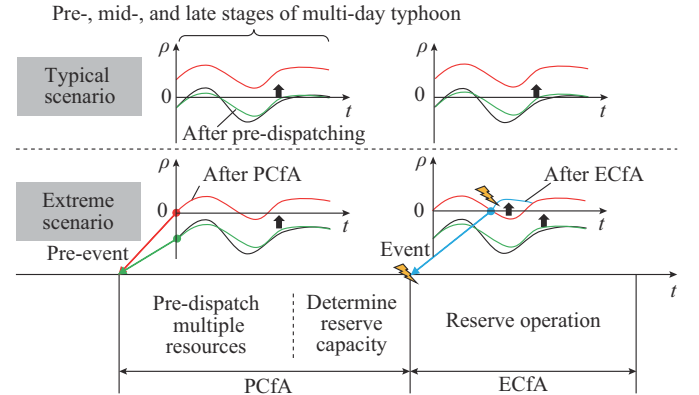


Fig. 2. Control strategies of PCfA and ECfA in typical and extreme scenarios.

In Fig. 2, the black curve is the initial adequacy of the power system. In the PCfA, the pre-dispatching strategies of multiple types of reserve resources including the fuel consumption pre-dispatching for thermal units, initial SOC pre-dispatching for energy storage system (ESS), and the pre-dispatching of interruption times for DSR resources, are proposed for coordinating different reserve resources before the extreme weather prediction, to adjust the adequacy in a longer time scale (i.e., the green curve in Fig. 2). Then, the reserve capacity in all stages of the multi-day typhoon can be optimized considering the reserve operation in multiple scenarios, to promote the adequacy of power systems (i.e., the red curve). To ensure the security of power systems after events (i.e., the blue curve), the reserve resources could be optimally operated for ECfA. In this paper, the medium- and short-term reserve arrangement optimization model is built with the optimization objective function of reducing

the comprehensive cost of PCfA, ECfA, and risks in multiple scenarios.

### A. Multi-scenario Stochastic Optimization Model of Reserve Arrangement

Based on the generated typical scenario set and the extreme scenario set considering the typhoon path – intensity prediction uncertainty, the multi-scenario stochastic optimization model of reserve arrangement can be built. In this model, the reserve capacity of multiple types of reserve resources during each time period under extreme weather is taken as the decision variable, to minimize the comprehensive cost of PCfA, ECfA, and risks. The objective function of the optimization model can be expressed as:

$$\min \left\{ \sum_{t=1}^T C_{P,t} + \sum_{s=1}^{N_s} p_s \sum_{t=1}^T (C_{E,t,s} + C_{K,t,s}) \right\} \quad (26)$$

$$C_{P,t} = C_{RC,t} + C_{TC,t} + C_{C,t} \quad (27)$$

$$C_{E,t,s} = C_{RE,t,s} + C_{TE,t,s} \quad (28)$$

where  $C_{P,t}$  is the PCfA cost at time  $t$  including the capacity cost of reserve  $C_{RC,t}$ , the cost of additional fuel purchasing and start-up/shut-down of thermal units  $C_{TC,t}$ , and the carbon emission cost  $C_{C,t}$ ;  $C_{E,t,s}$  is the ECfA cost at time  $t$  in scenario  $s$  including the electricity cost of reserve  $C_{RE,t,s}$  and the power system operation cost  $C_{TE,t,s}$ ; and  $C_{K,t,s}$  is the risk cost at time  $t$  in scenario  $s$ . Each type of cost in the objective function can be expressed as follows.

#### 1) PCfA Cost

The PCfA cost includes  $C_{RC,t}$ ,  $C_{TC,t}$ , and  $C_{C,t}$ , which can be expressed as:

$$C_{RC,t} = \sum_{i=1}^{N_T} \rho_{R,T_i}^u R_{T_i,t}^u + \sum_{i=1}^{N_S} \rho_{R,S_i}^u R_{S_i,t}^u + \sum_{i=1}^{N_D} \rho_{D_i,t} R_{D_i,t} + \sum_{i=1}^{N_T} \rho_{R,T_i}^d R_{T_i,t}^d + \sum_{i=1}^{N_S} \rho_{R,S_i}^d R_{S_i,t}^d \quad (29)$$

$$C_{TC,t} = \frac{1}{T} \sum_{i=1}^{N_T} (C_{B,T_i} - C_{F,T_i}) Q_{T_i}^B + \sum_{i=1}^{N_T} C_{SUSD,T_i} (v_{T_i,t} + z_{T_i,t}) \quad (30)$$

$$C_{C,t} = K_C (E_{r,t} - E_{l,t}) = K_C \left( F_{C,T_i} Q_{T_i,t} - \eta \sum_{i=1}^{N_T} P_{L_i,t} \right) \quad (31)$$

where  $\rho_{R,T_i}^u$  and  $\rho_{R,T_i}^d$  are the unit capacity costs of up and down reserves of thermal unit  $T_i$ , respectively;  $\rho_{R,S_i}^u$  and  $\rho_{R,S_i}^d$  are the unit capacity costs of up and down reserves of ESS  $S_i$ , respectively;  $\rho_{D_i,t}$  is the unit capacity cost of DSR resource  $D_i$  at time  $t$ ;  $R_{T_i,t}^u$  and  $R_{T_i,t}^d$  are the up and down reserve capacities of thermal unit  $T_i$  at time  $t$ , respectively;  $R_{S_i,t}^u$  and  $R_{S_i,t}^d$  are the up and down reserve capacities of ESS  $S_i$  at time  $t$ , respectively;  $R_{D_i,t}$  is the reserve capacity of DSR resource  $D_i$  at time  $t$ ;  $C_{B,T_i}$  is the additional fuel purchasing cost of thermal unit  $T_i$ ;  $C_{F,T_i}$  is the fuel purchasing cost in long-term market of thermal unit  $T_i$ ;  $Q_{T_i}^B$  is the additional purchased fuel of thermal unit  $T_i$ ;  $C_{SUSD,T_i}$  is the start-up/shut-down cost of thermal unit  $T_i$ ;  $v_{T_i,t}$  is the start-up state of thermal unit  $T_i$ ;  $z_{T_i,t}$  is the shut-down state of thermal unit  $T_i$ ;

$E_{r,t,s}$  is the carbon emissions of the total thermal units at time  $t$  in scenario  $s$ ;  $E_{l,t}$  is the regional carbon quota divided into time  $t$ ;  $K_C$  is the carbon emission price in carbon emission credit market;  $F_{C,T_i}$  is the carbon emission coefficient of thermal unit  $T_i$ ;  $Q_{T_i,t}$  is the fuel consumption of thermal unit  $T_i$  in scenario  $s$ ;  $P_{L_i,t}$  is the electricity load of load  $i$  at time  $t$ ; and  $\eta$  is the carbon quota coefficient.

#### 2) ECfA Cost

The ECfA cost includes  $C_{RE,t,s}$  and  $C_{TE,t,s}$ , which can be expressed as:

$$C_{RE,t,s} = \sum_{i=1}^{N_T} \rho_{E,T_i,t}^u P_{T_i,t,s}^u + \sum_{i=1}^{N_S} \rho_{E,S_i,t}^u P_{S_i,t,s}^u + \sum_{i=1}^{N_D} \rho_{E,D_i,t} P_{D_i,t,s} + \sum_{i=1}^{N_T} \rho_{E,T_i,t}^d P_{T_i,t,s}^d + \sum_{i=1}^{N_S} \rho_{E,S_i,t}^d P_{S_i,t,s}^d \quad (32)$$

$$C_{TE,t,s} = \sum_{i=1}^{N_T} C_{F,T_i} Q_{T_i,t,s} \quad (33)$$

where  $\rho_{E,T_i,t}^u$  and  $\rho_{E,T_i,t}^d$  are the unit electricity costs of up and down reserves of thermal unit  $T_i$  at time  $t$ , respectively;  $\rho_{E,S_i,t}^u$  and  $\rho_{E,S_i,t}^d$  are the unit electricity costs of up and down reserves of ESS  $S_i$  at time  $t$ , respectively;  $\rho_{E,D_i,t}$  is unit electricity cost of DSR resource  $D_i$  at time  $t$ ;  $P_{T_i,t,s}^u$  and  $P_{T_i,t,s}^d$  are the outputs of up and down reserves of thermal units  $T_i$  at time  $t$  in scenario  $s$ , respectively;  $P_{S_i,t,s}^u$  and  $P_{S_i,t,s}^d$  are the outputs of up and down reserves of ESS  $S_i$  at time  $t$  in scenario  $s$ , respectively;  $P_{D_i,t,s}$  is the reduced power of DSR resource  $D_i$  at time  $t$  in scenario  $s$ ; and  $Q_{T_i,t,s}$  is the fuel consumption of thermal unit  $T_i$  at time  $t$  in scenario  $s$ .

#### 3) Power System Risk Cost

The power system risk cost includes the expected cost of load loss and the expected cost of renewable energy curtailment, which can be expressed as:

$$C_{K,t,s} = E_{EENS,t,s} C_{VOLL} + E_{EEC,t,s} C_{VOC} \quad (34)$$

where  $E_{EENS,t,s}$  is the expected energy not supplied (EENS) at time  $t$  in scenario  $s$ ,  $E_{EENS,t,s} \geq 0$ ;  $C_{VOLL}$  is the VOLL;  $E_{EEC,t,s}$  is the expected energy curtailment (EEC) at time  $t$  in scenario  $s$ ,  $E_{EEC,t,s} \geq 0$ ; and  $C_{VOC}$  is the unit value of renewable energy curtailment.

The constraints of the multi-scenario stochastic optimization model of reserve arrangement include power balance constraints, which can be found in Supplementary Material A Section A.

### B. Reserve Pre-dispatching Model During Extreme Weather

#### 1) Pre-dispatching of Fuel Consumption of Thermal Unit Reserve Resources

In power systems with a high proportion of renewable energy sources, the thermal unit fuel stocks could be reduced, and the thermal units may not be started up for reducing the carbon emissions. In order to ensure the electricity reserve during extreme weather, the fuel stock of thermal units at the pre-, mid-, and late stages of typhoon could be pre-dispatched in this model. At the same time, affected by extreme weather, thermal units may not be able to replenish fuel stocks in a short time. Therefore, in order to prepare enough

fuel for power generation and reserve, additional fuel can be purchased before the extreme weather. The fuel consumption pre-dispatching strategy can be expressed as:

$$\begin{cases} Q_{T_i,t_0,d,s}^R \geq Q_{T_i,d,\min}^R \\ \sum_{t \in \mathbb{T}_E} Q_{T_i,t,s} \leq Q_{T_i,\mathbb{T}_E} + Q_{T_i}^B \end{cases} \quad (35)$$

$$Q_{T_i,t,s}^R = Q_{T_i,t-1,s}^R - Q_{T_i,t,s} \quad (36)$$

$$Q_{T_i,t,s} = a_{T_i} P_{T_i,t,s}^2 + b_{T_i} P_{T_i,t,s} + c_{T_i} \quad (37)$$

where  $Q_{T_i,t,s}^R$  is the remaining fuel of thermal unit  $T_i$  at time  $t$  in scenario  $s$ ;  $t_{0,d}$  is the initial time period of day  $d$ ;  $Q_{T_i,d,\min}^R$  is the minimum remaining fuel of thermal unit  $T_i$  pre-dispatched on day  $d$ ;  $\mathbb{T}_E$  is the set of time periods that the fuel supply is interrupted by extreme weather;  $Q_{T_i,\mathbb{T}_E}$  is the fuel stock of thermal unit  $T_i$  before time periods that the fuel supply is interrupted by extreme weather;  $P_{T_i,t,s}$  is the power of thermal unit  $T_i$  at time  $t$  in scenario  $s$ ; and  $a_{T_i}$ ,  $b_{T_i}$ , and  $c_{T_i}$  are the coefficients of the quadratic, primary, and constant terms of the quadratic function of fuel consumption, respectively. The quadratic function of fuel consumption can be linearized by piecewise linear fitting.

In the reserve arrangement optimization model, the reserve arrangements of thermal units at time  $t$  are decision variables, and the operation constraints of thermal unit reserve resources can be expressed as:

$$P_{T_i,t,s} = P_{T_i,t} + P_{T_i,t,s}^u - P_{T_i,t,s}^d \quad (38)$$

$$u_{T_i,t} P_{T_i,\min} \leq P_{T_i,t} \leq u_{T_i,t} P_{T_i,\max} \quad (39)$$

$$u_{T_i,t} P_{T_i,\min} \leq P_{T_i,t,s} \leq u_{T_i,t} P_{T_i,\max} \quad (40)$$

$$\begin{cases} R_{T_i,t}^u \geq P_{T_i,t,s}^u \geq 0 \\ R_{T_i,t}^d \geq P_{T_i,t,s}^d \geq 0 \end{cases} \quad (41)$$

where  $P_{T_i,t}$  is the fixed power of thermal unit  $T_i$  at time  $t$ ;  $P_{T_i,\max}$  and  $P_{T_i,\min}$  are the upper and lower generation limits of thermal unit  $T_i$ , respectively; and  $u_{T_i,t}$  is the commitment state of thermal unit  $T_i$  at time  $t$ . In addition, the other constraints of thermal units are the ramping up/down limits, up/down time limits, and  $N-1$  operating constraints, which can be seen in Supplementary Material A.

## 2) Pre-dispatching of Initial SOC of Energy Storage Reserve Resources

The ESS has fast and accurate response, which can reduce the required reserve capacity and the carbon emissions of thermal units. In the day-ahead dispatching model, the SOC of energy storage during the initial and end time periods of a day should be the same. In order to ensure the reserve of electricity during extreme weather, the energy storage device does not need to meet the SOC consistency constraint within a day in the initial SOC pre-dispatching model. According to the extreme weather prediction information, different lower limits of SOC are set on the day before, during, and after the typhoon, and the SOC of ESS during the initial and the end time periods of the week are set to be equal. Therefore, the initial SOC pre-dispatching model can be expressed as:

$$\begin{cases} S_{S_i,d,\min} \leq S_{S_i,t_0,d} \leq S_{S_i,d,\max} \\ S_{S_i,s,1} = S_{S_i,s,T} \end{cases} \quad (42)$$

where  $S_{S_i,t_0,d}$  is the SOC of ESS  $S_i$  on day  $d$ ; and  $S_{S_i,d,\max}$  and  $S_{S_i,d,\min}$  are the upper and lower limits, respectively.

In the reserve arrangement optimization model, the reserve arrangements of ESS at each time are decision variables, and the operation constraints of ESS reserve resources can be expressed as:

$$\begin{cases} 0 \leq P_{S_i,t,s}^u \leq R_{S_i,t}^u \\ 0 \leq P_{S_i,t,s}^d \leq R_{S_i,t}^d \end{cases} \quad (43)$$

$$P_{S_i,t,s}^{\text{cha}} = \max(P_{S_i,t}^{\text{cha}} - P_{S_i,t,s}^u + P_{S_i,t,s}^d, 0) \quad (44)$$

$$P_{S_i,t,s}^{\text{dis}} = \max(P_{S_i,t}^{\text{dis}} + P_{S_i,t,s}^u - P_{S_i,t,s}^d, 0) \quad (45)$$

$$S_{S_i,t,s} E_{S_i} = S_{S_i,t-1,s} E_{S_i} + \eta_{S_i}^{\text{cha}} P_{S_i,t,s}^{\text{cha}} - \frac{P_{S_i,t,s}^{\text{dis}}}{\eta_{S_i}^{\text{dis}}} \quad (46)$$

where  $P_{S_i,t,s}^{\text{cha}}$  and  $P_{S_i,t,s}^{\text{dis}}$  are the charging power and discharging power of ESS  $S_i$  at time  $t$  in scenario  $s$ , respectively;  $E_{S_i}$  is the capacity of ESS  $S_i$ ;  $\eta_{S_i}^{\text{cha}}$  and  $\eta_{S_i}^{\text{dis}}$  are the charging and discharging efficiencies of ESS  $S_i$ , respectively; and  $S_{S_i,t,s}$  is the SOC of ESS  $S_i$  at time  $t$  in scenario  $s$ . In addition, the other constraints of ESS are the charging and discharging constraints and SOC constraints, which can be found in Supplementary Material A.

## 3) DSR Resource Model Considering Pre-dispatching of Interruption Times and Reserve Reliability

With the promotion of load acquisition and control systems, DSR resources (interruptible loads, adjustable loads, translatable loads, and transferable loads) can cope with the requirements of the power system for resource diversification and cleaning, as well as dispatching intelligence and flexibility. The DSR resource model in this part is constructed taking interruptible loads as an example. In order to ensure the comfort of electricity users on the demand side, there is an upper limit to the number of interruptions of loads within a week. Therefore, the interruption times of loads on a single day in different stages of the typhoon could be pre-dispatched to achieve the coordination of DSR resources within a week. Therefore, the pre-dispatching of interruption times of DSR resources can be expressed as:

$$\begin{cases} \sum_{t=1}^T v_{D_i,t,s} \leq U_{D_i}^w \\ \sum_{t=t_{0,d}}^{t_d} v_{D_i,t,s} \leq U_{D_i,d,\max}^d \leq U_{D_i,\max}^d \end{cases} \quad (47)$$

where  $v_{D_i,t,s}$  is the interruption state of DSR resource  $D_i$  at time  $t$  of scenario  $s$ ;  $U_{D_i,\max}^w$  and  $U_{D_i,\max}^d$  are the upper limits of interruption times in the weekly time-scale and daily time-scale of DSR resource  $D_i$ , respectively; and  $U_{D_i,d,\max}^d$  is the pre-dispatched maximum interruption times on day  $d$  of DSR resource  $D_i$ .

In the reserve arrangement optimization model, the reserve arrangements of DSR resources at each moment are de-

cision variables, and the operation constraints of DSR resources can be expressed as:

$$u_{D_i,t,s} P_{D_i,\min} \leq P_{D_i,t,s} \leq u_{D_i,t,s} P_{D_i,\max} \quad (48)$$

$$R_{D_i,t} \geq P_{D_i,t,s} \geq 0 \quad (49)$$

where  $u_{D_i,t,s}$  is the commitment state of DSR resource  $D_i$  at time  $t$  in scenario  $s$ ; and  $P_{D_i,\min}$  and  $P_{D_i,\max}$  are the minimum and maximum interruptible capacities of DSR resource  $D_i$  at time  $t$  in scenario  $s$   $P_{D_i,t,s}$ , respectively. In addition, the other constraints of the DSR resource include interruption interval time limits and interruption duration limits, which can be found in Supplementary Material A.

The reliability of DSR resources is different from the thermal units and ESS, since there are some uncertainties in the user execution instructions and other processes of reserve operation. Therefore, considering the reliability difference of DSR resources, the  $N-x$  failure uncertainty set of DSR resources is constructed as:

$$L = \left\{ l \mid l_{i,t,s} \in \{0, 1\}, \prod_{j=1}^{N_D} \lambda_{D_j}^{l_{j,t,s}} \prod_{j=1}^{N_D} (1 - \lambda_{D_j})^{1-l_{j,t,s}} \geq \hat{\sigma}_{IL} \right\} \quad (50)$$

where  $\hat{\sigma}_{IL}$  is the total limit of the failure reliability; and  $\lambda_{D_i}$  is the reliability of DSR resource  $D_i$ . Since the  $N-x$  failure uncertainty model of DSR resources is nonlinear, the uncertainty set and power balance constraints can be linearized based on logarithm and robust dual transformation [41] as:

$$\left( \lg \hat{\sigma}_D - \sum_{i=1}^{N_D} \lg(1 - \lambda_{D_i}) \right) y_{t,s} - \sum_{i=1}^{N_D} z_{i,t,s} \geq \sum_{i=1}^{N_L} P_{L_i,t,s} - \sum_{i=1}^{N_T} P_{T_i,t,s} - \sum_{i=1}^{N_W} P_{W_i,t,s} - \sum_{i=1}^{N_G} P_{S_i,t,s}^{\text{dis}} + \sum_{i=1}^{N_G} P_{S_i,t,s}^{\text{cha}} - \sum_{i=1}^{N_D} P_{D_i,t,s} - E_{\text{EENS},t,s} + E_{\text{EWC},t,s} \quad (51)$$

$$(\lg \lambda_{D_i} - \lg(1 - \lambda_{D_i})) y_{t,s} - z_{i,t,s} \leq P_{D_i,t,s} \quad (52)$$

where  $y_{t,s}$  and  $z_{i,t,s}$  are the dual variables of the robust dual transformation, and  $y_{t,s} \geq 0$ ,  $z_{i,t,s} \geq 0$ .

Based on the linearization, an equivalent MILP model can be formulated and solved effectively through commercial tools. Overall, the flowchart of the risk-based coordination of medium- and short-term reserve arrangement is given in Fig. 3.

#### IV. CASE STUDIES

In this section, a simplified 24-node power system of Zhejiang province, China and the real typhoon data are utilized to verify the effectiveness of the proposed model. The topology of the simplified 24-node power system is shown in Supplementary Material B Fig. B1. The basic parameters, topological locations, and geographical locations of resources are shown in Tables BI-BIV. The data of typhoon Fireworks from July 24 to July 30 in 2021 based on the National Meteorological Center of China Meteorological Administration are used for the extreme scenario generation, and the predicted path, actual path, and extreme path based on the proposed model are shown in Supplementary Material B Fig. B2.

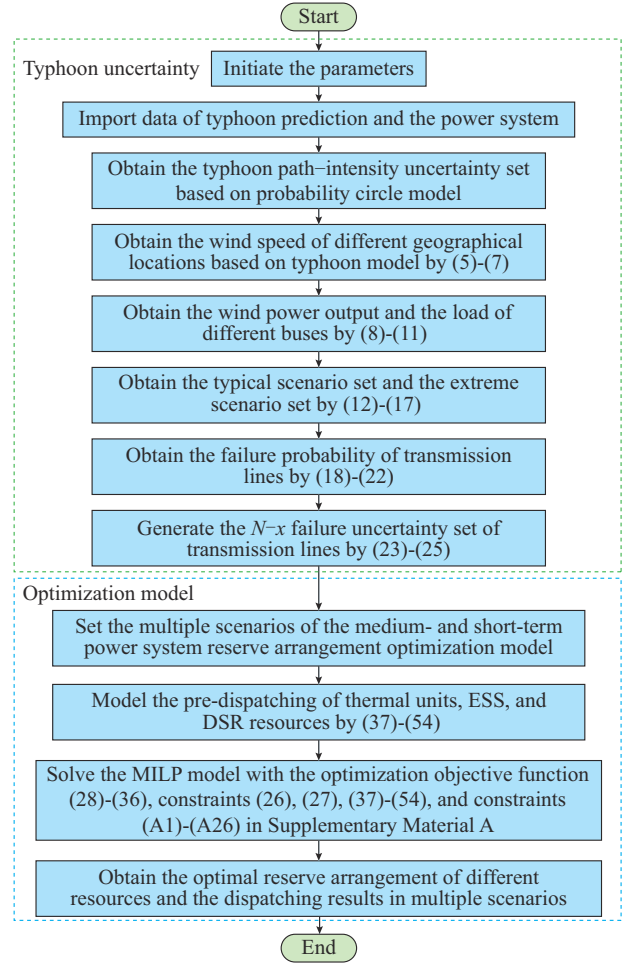


Fig. 3. Flowchart of risk-based coordination of medium- and short-term reserve arrangement.

The wind power and load data during normal weather are simulated based on the actual operation data of Zhejiang province, China. The optimization process is carried out on a PC with 16 GB of RAM and 3.60 GHz AMD Ryzen5 processor using Gurobi 9.5.0 solver and MATLAB 2019b, and the computation time is 25374 s.

#### A. Optimization Results

In this case, the optimal cost of the power system in multiple scenarios is expected to be \$301027, including \$199217 for PCfA cost, \$91911 for ECfA cost, and \$9899 for risk cost. The optimal operation results and reserve arrangement results of the different resources in the power system within a week (from July 24, 2021 to July 30, 2021) are shown in Supplementary Material C Fig. C1. Taking the periods during the typhoon (the 2<sup>nd</sup> day) and after the typhoon (the 7<sup>th</sup> day) as examples, the optimal results are shown in Fig. 4(a) and Fig. 4(b), respectively.

It can be observed from the typical and extreme NCP scenarios in Fig. 4 that both the variability between different typical scenarios and the fluctuations in extreme scenarios are amplified under typhoon disaster. The optimization results of the reserve arrangement indicate that the up-reserve requirement stays at a high level in both Fig. 4(a) and (b),

accounting for 12.6%-38.1% of the total load of the power system, which ensures the emergency reserve for  $N-1$  fault of the unit. Whereas the down-reserve requirement has significantly increased during the period greatly affected by the typhoon, from 8.4% to 21.45% on average. This is because the uncertainty of wind power output and load fluctuation increases when the typhoon lands and the reserve should be increased to reduce the operation risk. It can be observed from the actual typhoon scenario that the reserve arrangement optimization results can improve the operation adequacy in the actual typhoon scenario, without power load loss during all time periods. In addition, to further analyze the coordination strategy of different resources, the average reserve capacities of thermal units, ESS, and DSR resources during the peak load period (i.e., 00:00-08:00) and off-peak load period (i.e., 09:00-18:00) are shown in Fig. 5.

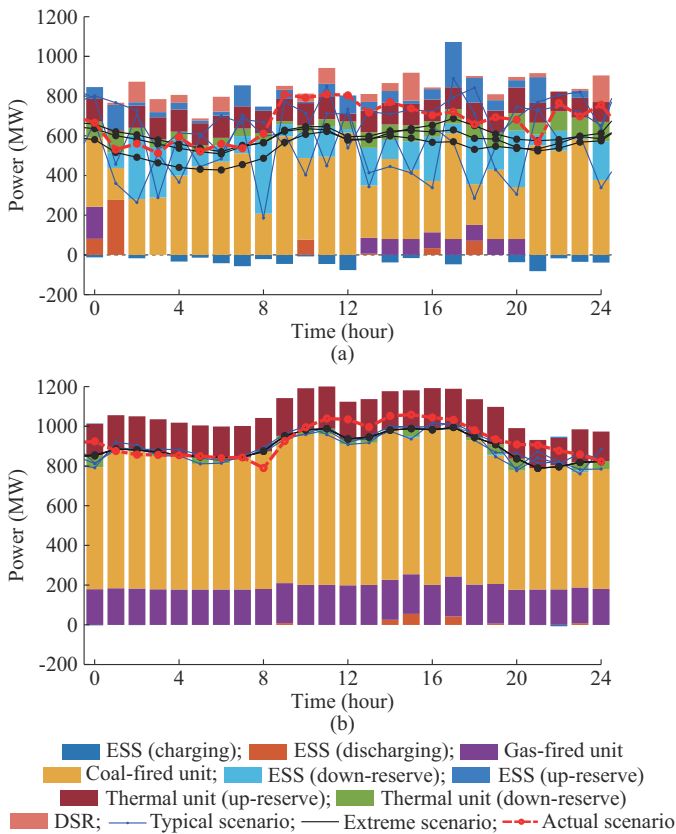


Fig. 4. Optimization results of optimal operation and reserve arrangement in power system. (a) The 2<sup>nd</sup> day. (b) The 7<sup>th</sup> day.

It can be observed from Fig. 5 that the reserve arrangement during the period less affected by the typhoon is mainly provided by the power generation resources, with the reserve capacity of thermal units, ESS, and DSR resources accounting for 91.7%, 7.8%, and 0.5% on average, respectively. On the other hand, the reserve arrangement of DSR resources and ESS significantly increases during the typhoon, with the reserve arrangement on the 2<sup>nd</sup>-4<sup>th</sup> days rising to 40.2%. Under typhoon disaster, the load of power systems is lower than that under normal conditions. Due to the minimum output constraints of thermal units, 72.7% of units are operational during the typhoon, compared with 85.2% under

normal conditions, resulting in reduced reserve capacity from thermal units. Concurrently, with increased fluctuation and higher failure probabilities of devices, the total reserve requirement of the power system has escalated. This has led to an increase in the reserve capacity provided by rapidly adjustable ESS and DSR resources. Specifically, the down-reserve capacity of ESS increases to 70.3% of the total down-reserve capacity on the 2<sup>nd</sup> day. To ensure the down-reserve capacity, the discharging electricity of ESS is 74.9 MWh on the 1<sup>st</sup> day, which pre-dispatches the SOC of ESS at the beginning of extreme weather to 0.1-0.2. Then, the reserve capacity on the 4<sup>th</sup> day is the highest due to a rebound in the power system load after typhoon, necessitating the pre-dispatching of DSR resources to ensure the availability of adequate reserve capacity, which is 40 MW during peak load period and 10 MW during off-peak load period, respectively.

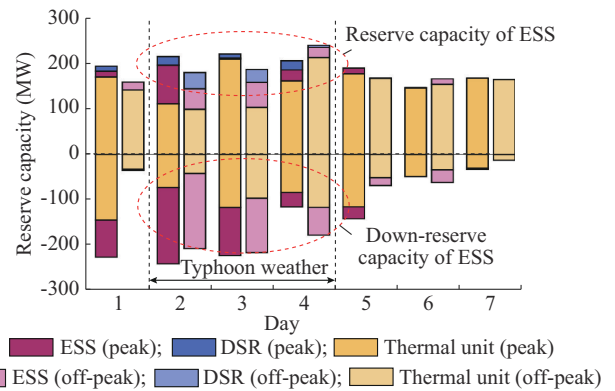


Fig. 5. Reserve arrangement during different time periods

To sum up, the proposed reserve arrangement optimization model can realize the spatio-temporal coordination of different resources in medium- and short-term, and improve the operation adequacy under the actual typhoon disaster.

### B. Impact of Typhoon Prediction Uncertainty on Reserve Arrangement Optimization

To verify the impact of considering the typhoon path-intensity prediction uncertainty on reserve arrangement optimization, the proposed model is compared with the scenario generation model that only considers the typhoon prediction center [10], and the actual typhoon scenario is utilized to verify the optimization results of different models. The scenario generation results of different models are shown in Supplementary Material C Fig. C2, and the costs of the power system under the actual typhoon disaster are shown in Table I.

TABLE I  
COSTS OF POWER SYSTEM UNDER ACTUAL TYPHOON DISASTER

Scenario generation model	Cost (\$10 <sup>4</sup> )				Proportion of reserve (%)		EENS (MWh)
	PCfA	ECfA	Risk	Total	Down	Up	
Proposed model	19.87	10.16	54.93	84.96	16.72	23.67	0
Without prediction uncertainty [10]	9.67	9.90	88.15	106.85	6.11	13.31	811.89

It can be observed from Fig. C2 that the NCP of multi-scenario generated in the proposed model fluctuates more widely during the time period of 48-96 hours, which can cover the actual scenario. The total cost of the power system under the actual typhoon disaster is reduced by 20.4% compared with that without considering the typhoon path-intensity prediction uncertainty. Since the actual path of the typhoon is on the right side of the typhoon prediction center (as shown in Fig. B2), the deviation of renewable energy and load prediction increases. For example, the impact on the wind generation  $W_2$  in Table BI delay from the expected time, and the intensity of the typhoon is larger than that in the prediction. It can be observed from Table I that the optimal reserve arrangement increases in the model considering the typhoon prediction uncertainty, and the up- and down-reserve capacities increase by 10.5%. As a result, the PCfA cost increases from \$96700 to \$19870, while the risk cost decreases from \$881500 to \$549300. To sum up, the adequacy of the power system could be improved and the loss of load under a typhoon disaster could be reduced when the typhoon prediction uncertainty is fully considered.

### C. Comparison with Other Reserve Arrangement Optimization Models

To illustrate its advantages, the proposed model (M-SMT) is compared with the short-term reserve arrangement optimization model (M-ST)[23], the reserve requirement determination model based on the  $N-1$  event of the power system (M- $N-1$ ) [14] and  $N-2$  events (M- $N-2$ ), and the polytopic-based reserve arrangement optimization model (M-PB) [42]. The total optimal costs of the power system in M-ST, M- $N-1$ , M- $N-2$ , and M-PB are \$698466, \$367569, \$365912, and \$374691, respectively, and that in the proposed model is \$301027. Therefore, compared with the M-ST, M- $N-1$ , M- $N-2$ , and M-PB, the total optimal cost of the power system in multiple scenarios of the proposed model can be reduced by 56.9%, 18.1%, 17.7%, and 19.7%, respectively. The optimization results and the optimal cost in multiple scenarios of each model are shown in Fig. 6.

#### 1) Effect of Medium- and Short-term Reserve Coordination

It can be observed from Fig. 6 that compared with the M-ST, which does not consider the pre-scheduling of different reserve resources, the proposed model can guarantee the power system security and reduce ECfA cost through the lightly increase of PCfA cost. The total PCfA cost in the proposed model is \$199217, which is 11.9% higher than that in the M-ST, while the ECfA cost and risk cost are significantly reduced from \$641958 to \$91911 and from \$23630 to \$9899, respectively. In particular, it is difficult to maintain a reasonable level of system reserve on the 4<sup>th</sup> day of the week in the M-ST, which leads to an increase in the risk of load loss and risk of renewable energy curtailment on that day, resulting in a significant increase in the total cost of the power system. The interruption times of DSR resources D1-D8 and fuel stocks of thermal units  $T_1$ - $T_8$  from the 2<sup>nd</sup> to the 4<sup>th</sup> days in the M-ST and the proposed model are shown in Fig. 7 and Fig. 8, respectively.

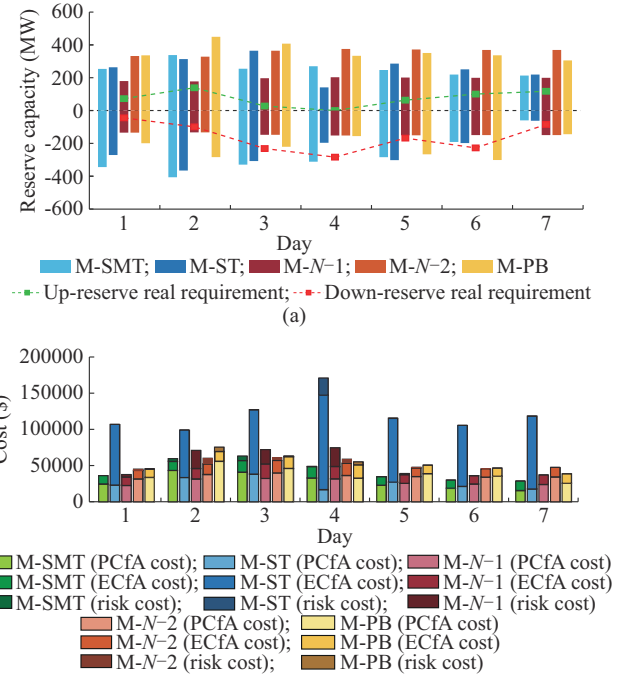


Fig. 6. Comparison of optimization results and optimal cost of different reserve arrangement optimization models. (a) Optimization results of reserve arrangement. (b) Optimal cost in multiple scenarios.

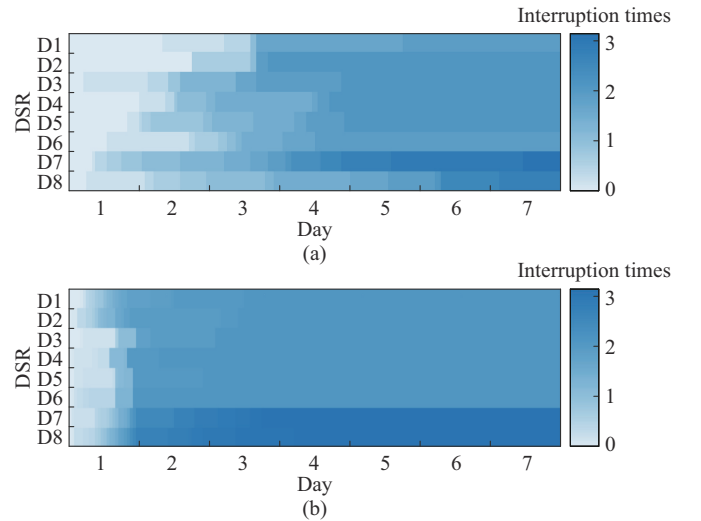


Fig. 7. Interruption times of DSR resources with different reserve arrangement optimization models. (a) M-SMT. (b) M-ST.

It can be observed in Fig. 7 that the arrangement of DSR resources is concentrated during extreme weather periods in the proposed model, and there is also pre-dispatching of some interruption times during the period of load rising after typhoon. In the M-ST, the arrangement of DSR resources is concentrated on the first two days of the week, and the upper limit of interruption times of each DSR resource is reached at hour 63, so there is a lack of DSR resources in the late stage of extreme weather. Therefore, a more reasonable scheduling result of interruption times can be obtained in the proposed model compared with that in the M-ST. It can be observed from Fig. 8(a) that it is more reasonable to optimize the combination of thermal units through the proposed model. For example, thermal unit  $T_2$  is shut down on

the 1<sup>st</sup> day of extreme weather, whereas thermal unit  $T_1$  is shut down on the 2<sup>nd</sup> day of extreme weather so that the fuel stocks on the 3<sup>rd</sup> day can guarantee the power generation and reserve requirements. However, it can be observed from Fig. 8(b) that most of the thermal units start up on the first two days of extreme weather. Although the reserve resources in the initial stage of extreme weather are sufficient, there is a shortage of electricity reserve resources in the late stage of extreme weather, which increases the risk of load loss and renewable energy curtailment. The medium- and short-term reserve arrangement optimization can reduce the risk of the shortage of fuel supply to the power generation and the insufficient interruption times of DSR resources.

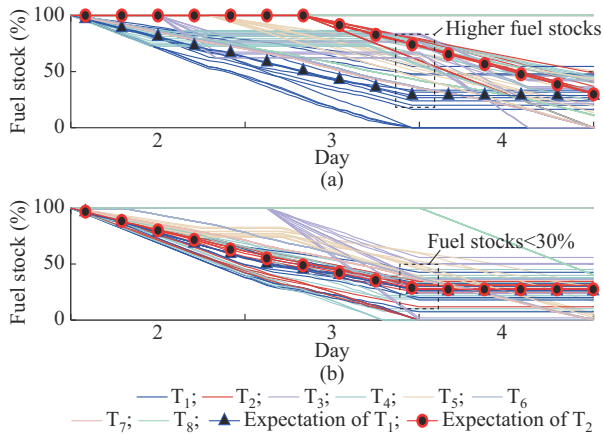


Fig. 8. Fuel stocks of thermal units from the 2<sup>nd</sup> to the 4<sup>th</sup> days with different reserve arrangement optimization models. (a) M-SMT. (b) M-ST.

## 2) Effect of Multi-scenario Stochastic Optimization

It can be observed from Fig. 6 that compared with the M-N-1, M-N-2, and M-PB, the proposed model can coordinate PCfA and ECfA costs in different stages of extreme weather, reducing the cost and risk during extreme weather. The PCfA and ECfA costs of the proposed model (\$199217 and \$91911) are approximately the same as those of the M-N-1 (\$192300 and \$99827), while the risk cost is significantly reduced from \$75442 to \$9899. This is because the reserve arrangement on the 5<sup>th</sup>-7<sup>th</sup> days and in the off-peak load period is decreased to reduce the cost of prevention control, while the reserve arrangement on the 1<sup>st</sup>-4<sup>th</sup> days and in the peak load period is increased to ensure power system security. In the M-N-2 and M-PB, the power system security can also be promoted without risks, but the PCfA costs in the optimization result are \$249366 and \$268543, respectively, which are 20.1% and 25.8% greater than that in the proposed model. Therefore, the multi-scenario stochastic optimization of the medium- and short-term reserve arrangement during extreme weather can reduce the prevention control cost on the premise of ensuring power system security.

## V. CONCLUSION

In this paper, the medium- and short-term reserve arrangement optimization for multiple types of reserve resources considering typhoon uncertainty is studied. Considering the typhoon path-intensity prediction uncertainty and reserve ar-

range adequacy control, a reserve arrangement optimization model is constructed with the goal of minimizing the total cost of power system reserve and operation in multiple scenarios. Case studies are performed on an actual power system with real typhoon data, and the following conclusion can be obtained by the simulation and comparison.

1) The typhoon path-intensity prediction uncertainty is fully considered in the proposed extreme scenario generation and reduction method based on the typhoon double probability circle model. The adequacy of the power system could be improved by 10.5% and the loss of load under the typhoon disaster could be reduced (from 811.89 MWh to 0 in the actual typhoon scenario) compared with the scenario generation model that only considers the typhoon center prediction.

2) The medium- and short-term reserve arrangement optimization model can reduce the risk of the shortage of fuel supply on the power generation and the insufficient interruption times of DSR resources during predictable extreme weather. The risk cost of the proposed model is significantly reduced from \$23630 to \$9899 compared with that of the M-ST.

3) The reserve arrangement optimization model considering typhoon uncertainty coordinates PCfA and ECfA costs during extreme weather. Compared with the M-N-1, M-N-2, and M-PB, the proposed model can reduce the prevention control cost on the premise of ensuring power system security, and the combined cost can be reduced by an average of 18.5%.

## REFERENCES

- [1] M. Cao and J. Yu, "Dynamic setting method of assessment indicators for power curves of renewable energy sources considering scarcity of reserve resources," *Journal of Modern Power Systems and Clean Energy*, vol. 12, no. 1, pp. 101-114, Jan. 2024.
- [2] I. F. Abidin, Y.-P. Fang, and E. Zio, "A modeling and optimization framework for power systems design with operational flexibility and resilience against extreme heat waves and drought events," *Renewable and Sustainable Energy Reviews*, vol. 112, pp. 706-719, Sept. 2019.
- [3] C. Zhang, L. Liu, H. Cheng *et al.*, "Frequency-constrained co-planning of generation and energy storage with high-penetration renewable energy," *Journal of Modern Power Systems and Clean Energy*, vol. 9, no. 4, pp. 760-775, Jul. 2021.
- [4] N. G. Paterakis, M. Gibescu, A. G. Bakirtzis *et al.*, "A multi-objective optimization approach to risk-constrained energy and reserve procurement using demand response," *IEEE Transactions on Power Systems*, vol. 33, no. 4, pp. 3940-3954, Jul. 2018.
- [5] J. Wang, N. Xie, C. Huang *et al.*, "Two-stage stochastic-robust model for the self-scheduling problem of an aggregator participating in energy and reserve markets," *Protection and Control of Modern Power Systems*, vol. 8, no. 3, pp. 1-20, Jul. 2023.
- [6] S. Veda, Y. Zhang, J. Tan *et al.*, "Evaluating the impact of the 2017 solar eclipse on US western interconnection operations," Tech. Rep., National Renewable Energy Laboratory (NREL), Golden, USA, Apr. 2018.
- [7] Y. Xue, D. Xie, F. Xue *et al.*, "A research framework for operation adequacy in smart grid, part I: elements and models," *Automation of Electric Power Systems*, vol. 38, no. 10, pp. 1-9, May 2014.
- [8] B. Cai, Y. Xue, F. Xue *et al.*, "A research framework for operation adequacy in smart grid, part II: problems and ideas," *Automation of Electric Power Systems*, vol. 38, no. 11, pp. 1-6, Jun. 2014.
- [9] B. Cai, Y. Xue, F. Xue *et al.*, "A research framework for operation adequacy in smart grid, part III: decoupling and coordination," *Automation of Electric Power Systems*, vol. 38, no. 12, pp. 1-5, Jun. 2014.
- [10] H. Khaloie, A. Abdollahi, M. Rashidinejad *et al.*, "Risk-based probabilistic-possibilistic self-scheduling considering high-impact low-probability events uncertainty," *International Journal of Electrical Power & Energy Systems*, vol. 110, pp. 598-612, Sept. 2019.
- [11] H. Liu, C. Wang, P. Ju *et al.*, "A sequentially preventive model en-

- hancing power system resilience against extreme-weather-triggered failures,” *Renewable and Sustainable Energy Reviews*, vol. 156, p. 111945, Mar. 2022.
- [12] T. Ding, M. Qu, Z. Wang *et al.*, “Power system resilience enhancement in typhoons using a three-stage day-ahead unit commitment,” *IEEE Transactions on Smart Grid*, vol. 12, no. 3, pp. 2153-2164, May 2021.
- [13] Z. Wang, T. Ding, W. Jia *et al.*, “Multi-stage stochastic programming for resilient integrated electricity and natural gas distribution systems against typhoon natural disaster attacks,” *Renewable and Sustainable Energy Reviews*, vol. 159, p. 111784, May 2022.
- [14] ERCOT. (2023, Apr.). Protocols Section 6. [Online]. Available: [https://www.ercot.com/content/wcm/libraries/151823/April\\_11\\_2018\\_Nodal\\_Protocols.pdf](https://www.ercot.com/content/wcm/libraries/151823/April_11_2018_Nodal_Protocols.pdf)
- [15] PJM. (2023, Feb.). M-11. [Online]. Available: <https://www.pjm.com/-/media/documents/manuals/m11.ashx>
- [16] J. Dowell, G. Hawker, K. Bell *et al.*, “A review of probabilistic methods for defining reserve requirements,” in *Proceedings of 2016 IEEE PES General Meeting*, Boston, USA, Jul. 2016, pp. 1-5.
- [17] Z. Zhou and A. Botterud, “Dynamic scheduling of operating reserves in co-optimized electricity markets with wind power,” *IEEE Transactions on Power Systems*, vol. 29, no. 1, pp. 160-171, Jan. 2014.
- [18] M. Bucksteeg, L. Nielsen, and C. Weber, “Impacts of dynamic probabilistic reserve sizing techniques on reserve requirements and system costs,” *IEEE Transactions on Sustainable Energy*, vol. 7, no. 4, pp. 1408-1420, Oct. 2016.
- [19] I. Krad, D. W. Gao, and H. Wu, “An assessment of flexibility reserves in stochastic modeling at multiple timescales,” *CSEE Journal of Power and Energy Systems*, vol. 3, no. 1, pp. 84-92, Mar. 2017.
- [20] V. Dvorkin, S. Delikaraoglou, and J. M. Morales, “Setting reserve requirements to approximate the efficiency of the stochastic dispatch,” *IEEE Transactions on Power Systems*, vol. 34, no. 2, pp. 1524-1536, Mar. 2019.
- [21] B. Park, Z. Zhou, A. Botterud *et al.*, “Probabilistic zonal reserve requirements for improved energy management and deliverability with wind power uncertainty,” *IEEE Transactions on Power Systems*, vol. 35, no. 6, pp. 4324-4334, Nov. 2020.
- [22] A. Papavasiliou, A. Bouso, S. Apelfröjd *et al.*, “Multi-area reserve dimensioning using chance-constrained optimization,” *IEEE Transactions on Power Systems*, vol. 37, no. 5, pp. 3982-3994, Sept. 2022.
- [23] S. Lu, Y. Wu, S. Lou *et al.*, “A model for optimizing spinning reserve requirement of power system under low-carbon economy,” *IEEE Transactions on Sustainable Energy*, vol. 5, no. 4, pp. 1048-1055, Oct. 2014.
- [24] S. Lou, S. Lu, Y. Wu *et al.*, “Optimizing spinning reserve requirement of power system with carbon capture plants,” *IEEE Transactions on Power Systems*, vol. 30, no. 2, pp. 1056-1063, Mar. 2015.
- [25] C. Lv, R. Liang, W. Jin *et al.*, “Multi-stage resilience scheduling of electricity-gas integrated energy system with multi-level decentralized reserve,” *Applied Energy*, vol. 317, p. 119165, Jul. 2022.
- [26] A. A. Taylor and B. Glahn. (2008, Jan.). Probabilistic guidance for hurricane storm surge. [Online]. Available: [https://www.researchgate.net/publication/237559129\\_Probabilistic\\_guidance\\_for\\_hurricane\\_storm\\_surge](https://www.researchgate.net/publication/237559129_Probabilistic_guidance_for_hurricane_storm_surge)
- [27] H. Hasegawa, N. Kohno, and H. Hayashibara. (2012, Jan.). JMA’s storm surge prediction for the WMO storm surge watch scheme (SS-WS). [Online]. Available: <https://www.jma.go.jp/jma/eng/jma-center/rsmc-hp-pub-eg/techrev/text14-2.pdf>
- [28] W. Guo, B. An, C. Qiu *et al.*, “Probabilistic forecast for typhoon storm surge based on multi-source data: creation of typhoon ensemble,” *Marine Forecasts*, vol. 38, no. 1, pp. 26-33, Feb. 2021.
- [29] Y. Wu, Y. Xue, Y. Xie *et al.*, “Space-time impact of typhoon and rain-storm on power grid fault probability,” *Automation of Electric Power Systems*, vol. 40, no. 2, pp. 20-29, Jan. 2016.
- [30] M. Miyazaki, “Studies on storm surges and tides,” *Journal of the Oceanographical Society of Japan*, vol. 36, pp. 163-166, Aug. 1980.
- [31] Z. Wu, L. Zhao, Y. Ge *et al.*, “Statistics on the joint probability distribution of wind speed and rain intensity under typhoon conditions in Shanghai,” *Acta Aerodynamica*, vol. 28, no. 4, pp. 393-399, Aug. 2010.
- [32] P. Umamathy, V. Chinthakunta, and S. A. Muthukumaraswamy, “Assessment of available transfer capability incorporating probabilistic distribution of load using interval arithmetic method,” *International Journal of Computer and Electrical Engineering*, pp. 692-697, vol. 2, no. 4, pp. 692-697, Jan. 2010.
- [34] H.-S. Park and C.-H. Jun, “A simple and fast algorithm for  $K$ -medoids clustering,” *Expert Systems with Applications*, vol. 36, no. 2, pp. 3336-3341, Mar. 2009.
- [35] B. Li, J. Sun, P. Yu *et al.*, “A multi-dimensional typical scenarios generation algorithm for distribution network based on load clustering and network structure equivalence,” *Proceedings of the CSEE*, vol. 41, no. 8, pp. 2661-2671, Apr. 2021.
- [36] X. Liu, K. Hou, H. Jia *et al.*, “A Planning-oriented resilience assessment framework for transmission systems under typhoon disasters,” *IEEE Transactions on Smart Grid*, vol. 11, no. 6, pp. 5431-5441, Nov. 2020.
- [37] Z. Qin, X. Chen, Y. Hou *et al.*, “Coordination of preventive, emergency and restorative dispatch in extreme weather events,” *IEEE Transactions on Power Systems*, vol. 37, no. 4, pp. 2624-2638, Jul. 2022.
- [38] P. A. Trodden, W. A. Bukhsh, A. Grothey *et al.*, “Optimization-based islanding of power networks using piecewise linear AC power flow,” *IEEE Transactions on Power Systems*, vol. 29, no. 3, pp. 1212-1220, May 2014.
- [39] T. Zhao, H. Zhang, X. Liu *et al.*, “Resilient unit commitment for day-ahead market considering probabilistic impacts of hurricanes,” *IEEE Transactions on Power Systems*, vol. 36, no. 2, pp. 1082-1094, Mar. 2021.
- [40] Y. Yang, M. Bao, Y. Ding *et al.*, “Impact of down spinning reserve on operation reliability of power systems,” *Journal of Modern Power Systems and Clean Energy*, vol. 8, no. 4, pp. 709-718, Jul. 2020.
- [41] Q. Wang, J.-P. Watson, and Y. Guan, “Two-stage robust optimization for  $N-k$  contingency-constrained unit commitment,” *IEEE Transactions on Power Systems*, vol. 28, no. 3, pp. 2366-2375, Aug. 2013.
- [42] S. Khan, W. Gawlik, and P. Palensky, “Reserve capability assessment considering correlated uncertainty in microgrid,” *IEEE Transactions on Sustainable Energy*, vol. 7, no. 2, pp. 637-646, Apr. 2016.

**Yunchu Wang** received the B.E. degree in electrical engineering from Zhejiang University, Hangzhou, China, in 2020. She is currently pursuing the Ph.D. degree with the College of Electrical Engineering, Zhejiang University. Her research interests include power system economics and optimization, and demand response.

**Yusheng Xue** received the Ph.D. degree from the University of Liege, Liege, Belgium, in 1987. He has been an Academician with the Chinese Academy of Engineering since 1995. He is currently the Honorary President of the State Grid Electric Power Research Institute (SGEPRI), Nanjing, China, an Adjunct Professor in dozens of Chinese universities, and an Adjunct Professor with the University of Newcastle, Newcastle, Australia. He is the Editor-in-Chief of the *Automation of Electric Power System* (in Chinese) and the *Journal of Modern Power Systems and Clean Energy*, as well as the Chairman of the Technical Committee of Chinese National Committee of CIGRE since 2005. His research interest includes power system automation.

**Dongliang Xie** received the Ph.D. degree in electrical engineering from Southeast University, Nanjing, China, in 2012. During 2011-2012, he was a Research Associate in Hong Kong Polytechnic University, Hong Kong, China. He is currently working for State Grid Electric Power Research Institute (SGEPRI), Nanjing, China. His research interests include analysis, simulation and control for smart grid architectures and essentials consisting of renewable power generation, power market and power system interaction, and demand elasticity.

**Yuge Chen** received the B.E. degree in electrical engineering from Fuzhou University, Fuzhou, China, in 2020, and the M.E. degree from Zhejiang University, Fuzhou, China, in 2023. Her research interests include power system restoration, configuration and scheduling optimization of virtual power plants, and shared energy storage technology.

**Changming Chen** received the B.E. degree in electrical engineering from Fuzhou University, Fuzhou, China, in 2019. He is currently pursuing the Ph.D. degree with the College of Electrical Engineering, Zhejiang University, Hangzhou, China. His research interests include power system restoration, configuration and scheduling optimization of integrated energy systems, and shared energy storage technology.

**Zhenzhi Lin** received the Ph.D. degree in electrical engineering from the South China University of Technology, Guangzhou, China, in 2008. From 2007 to 2008, he was a Research Assistant with the Department of Electrical Engineering, The Hong Kong Polytechnic University, Hong Kong, China, a Research Scholar with the Department of Electrical Engineering and Computer Science, University of Tennessee, Knoxville, USA, from 2010 to 2011, and a Research Associate with the College of Engineering and Computing Sciences, Durham University, Durham, U.K., from 2013 to 2014. He is currently a Professor with the College of Electrical Engineering, Zhejiang University, Hangzhou, China. His research interests include power system situational awareness, power system restoration, power system economics, data mining, and artificial intelligence application in power systems.